

Appendix A

**Finite Element Stress
Analysis of Davis-Besse
CRDM Nozzle 3
Penetration**

Appendix A Finite Element Stress Analysis of Davis-Besse CRDM Nozzle 3 Penetration

Exponent developed a three-dimensional finite element model of the control rod drive mechanism (CRDM) Nozzle-3 penetration in the Davis Besse reactor pressure vessel (RPV) head for evaluation of weld residual and operational stresses in and around the J-groove weld. The modeled loading history included the buttering deposit, nozzle expansion, thirteen weld passes, the hydrostatic test and normal operating conditions. The stress results can be used to predict crack growth in the nozzle wall.

Finite Element Model

The finite element model of the Nozzle-3 penetration, shown in Figure A.1, represents a portion of the hemispherical head extending half the distance from Nozzle 3 to neighboring Nozzles 1, 6 and 11. Advantage was taken of a plane of geometrical symmetry passing through the nozzle centerline along a meridian of the hemispherical RPV head. This plane of symmetry allowed for simulation of the full nozzle using a model representing only half of the nozzle. Appropriate boundary conditions applied on the symmetry (or cut) plane cause the half-symmetry model to behave just like the full nozzle. This common modeling technique optimizes solution efficiency by avoiding redundant calculations.

The finite element model was developed from dimensional information obtained from the following Babcock & Wilcox (B&W) fabrication drawings and quality control records:

- Drawing No. 154632 E2¹
- Drawing No. 154631 E4²
- Drawing No. 154628 E5³
- Quality Control Inspection Drawing No. 156631 E-R2⁴

- Quality Control Inspection Drawing No. 154628 E4⁵

Unlike most other similar B&W reactors, the Davis-Besse head was fabricated without counter bores in the CRDM nozzle penetrations⁶. This means that the nozzle shrink-fit interference was not uniform around the circumference of the nozzle due to the curvature of the head. The interference contact zone extended higher on the nozzle on the uphill side and lower on the nozzle on the downhill side.

Material Properties

Four different materials models were used in the analysis. In each case, material properties such as the conductivity, specific heat, thermal expansion coefficient, elastic modulus and strength data were modeled as a function of temperature.

The hemispherical head was modeled as ASME SA-533, Grade B, Class 1 alloy steel. The properties were taken from the ASME Boiler and Pressure Vessel Code⁷. The elastic modulus is given as a function of temperature in Figure A.3, the specific heat as a function of temperature in Figure A.4, the thermal conductivity as a function of temperature in Figure A.5, the thermal expansion as a function of temperature in Figure A.6 and strength as a function of the temperature in Figure A.7. The head material was modeled as elastic-perfectly plastic with temperature-dependent yield strength based on the yield curve in Figure A.7. The input stress-strain relations for the head material are shown in Figure A.8.

The cladding on the inside of the head is modeled as Type 308 stainless steel. The elastic modulus as a function of temperature is given in Figure A.9. Yield, tensile, and flow stress as a function of temperature for Type 308 stainless steel cladding is given in Figure A.10. Poisson's ratio was taken as 0.29 over the entire temperature range. The density of Type 308 stainless steel is 499.4 lb/ft³. The thermal expansion coefficient as a function of temperature is shown in Figure A.11, the specific heat as a function of temperature in Figure A.12 and the thermal conductivity as a function of temperature in Figure A.13.

The nozzle is modeled as the nickel-chrome-iron alloy Inconel 600. The stress-strain data for Inconel 600 was adapted from the ASME Code and Special Metals product brochures. The 0.2%-offset yield points were taken from Special Metals data and Heat M3935 Cert. The stress-strain data of Alloy 600 at 2300°F was taken from EPRI TR-103696, Fig. 7-3. The final input stress-strain curves are shown in Figure A.14. Elastic modulus as a function of temperature was taken from the ASME Code and is shown in Figure A.15 and Poisson's ratio as a function of temperature is shown in Figure A.16. Temperature-dependent thermal properties for Inconel 600 were obtained from the ASME Code. The coefficient of thermal expansion is given in Figure A.17, the thermal conductivity in Figure A.18, the specific heat in Figure A.19 and the emissivity Figure A.20. Density varies little with temperature, so a constant value of 528.8 lb/ft³ was used.

The J-groove weld and buttering was modeled as Inconel 182 (Alloy 182) weld filler metal. The thermal and elastic properties of the weld filler metal are the same as the INCONEL Alloy 600 properties. The work hardening behavior for Inconel 182 is shown in Figure A.21.

Loading History

The Davis-Besse RPV head assembly was fabricated in a number of steps. Several key steps influenced the stress states in and around the CRDM nozzle J-groove welds. The hemispherical alloy-steel head was clad on the inside with a layer of Type 308 stainless steel weld metal. Following this, the CRDM nozzle penetrations were bored through the head and cladding. Then the J-grooves were cut on the inside end of each CRDM penetration to accept the multi-pass welds which join the CRDM nozzles to the head and create a watertight seal. The surface of the J-grooves was then "buttered" (or clad) with a layer of Alloy 182 weld metal. At this point, the entire head was given a thermal stress relief treatment at 1125°F. The CRDM nozzles were matched to the head penetrations and each was ground to final dimensions that provided a targeted interference fit of 0.0013 to 0.0015 inch. To install each slightly oversized nozzle into its head penetration, the nozzle was cooled to around -320°F in liquid nitrogen to shrink it and then inserted into the penetration. As the nozzle warmed to ambient temperature, it expanded into

contact with the head, locking it in position. Lastly, the multi-pass J-groove welds were applied to join the nozzles with the head and provide a watertight seal.

There was no post-welding thermal stress relief treatment given to the head after the J-groove welds were applied. Therefore, tensile residual stresses from weld cooling remained in and around the J-groove welds after head assembly fabrication. Prior to service, the entire reactor pressure vessel must pass an ASME-Code required hydrostatic pressure test to 3,125 psi (1.25 times its design pressure of 2,500 psi). This pressure test leads to some localized yielding in and around the J-groove welds due to their already high tensile residual stresses from welding. This yielding during the pressure test results in a slight reduction in the residual stresses.

In service, the reactor pressure vessel was subjected to the full-load operational pressure and temperature of the primary cooling water. During Cycle 13 at Davis-Besse, the RCS pressure averaged about 2155 psi and the temperature averaged just over 605°F.

The finite element model of Nozzle 3 was analyzed in the following steps to simulate the actual sequence of fabrication, testing, and operational loading:

- solidification and cooling of the J-groove weld buttering from 2240°F to 70°F,
- stress relief of the head, cladding, and J-groove buttering at 1125°F,
- cooling of the nozzle to -320°F, installation of the nozzle into the head, and warming of the nozzle back to 70°F to achieve the interference fit,
- sequential application of thirteen weld passes, each deposited at 2240°F and cooled below a maximum inter-pass temperature of 350°F,
- pressurization of the wetted internal surfaces up to the hydrostatic test pressure of 3,125 psi and back to zero pressure, and

- pressurization to the operating pressure of 2,155 psi at a temperature of 605°F.

Throughout the simulation, the boundary planes of the modeled head segment were constrained to allow only radial displacement. Such boundary conditions cause the model to behave as if it were part of the complete hemispherical head.

The analysis of the Nozzle-3 model involved both transient thermal and thermal-mechanical solutions. A coupled analysis technique was employed wherein a transient thermal solution and a thermal-mechanical solution is obtained for each small increment of load application. This type of incremental coupled analysis was necessary to appropriately simulate the nonlinear response (in both stress and displacement) of the nozzle to temperature and pressure loads.

J-groove Weld Buttering

To simulate the buttering weld deposit and cool down, the elements representing the buttering were initially set to 2240°F. The remote cut boundaries of the truncated head portion of the model were held at 70°F during the weld deposition and cool down stages. Radiation boundary conditions were applied to the exposed faces of the buttering. Convective boundary conditions were applied to the exposed faces of the buttering and the top and bottom faces of the head. For both the head and nozzle, turbulent free convective film coefficients were used with an ambient-air sink temperature of 70°F. Heat was also allowed to conduct away from the weld through the head. The buttering weld was allowed to cool to near ambient temperature. During the buttering analysis, the nozzle portion of the model was deactivated to simulate the fact that the nozzle was not yet installed.

Head Stress Relief

After the buttering step, the temperature of the entire model was raised uniformly to the stress-relief temperature of 1125°F and then reduced back to 70°F. Since the yield strength of the materials is lower at higher temperatures, this step reduced the residual stresses around the buttering weld. However, the stress relief does not remove all

residual stress from the head, and the buttering and head cladding layers remained in tension after this step.

Nozzle Installation with Interference Fit

Following the stress relief step, the nozzle portion of the model was activated and shrunk by cooling to -320°F . Frictional contact interfaces on the outside of the nozzle and the inside of the head penetration bore were activated, and the nozzle was warmed back to 70°F , engaging contact between the nozzle and head to accurately simulate the interference fit. The coefficient of friction between the head and nozzle was taken as 0.2. At the end of the nozzle heating, there was complete contact between the nozzle and head.

J-groove Weld Deposition

After the nozzle heat up, the thirteen weld passes were deposited sequentially starting at the root of the J-groove. The elements representing each weld pass were activated at 2240°F and allowed to cool to below 350°F before the next pass was deposited. The boundaries of the truncated head portion of the model remote from the nozzle were again held at 70°F for these thermal loading steps. Radiation boundary conditions were applied to the exposed faces of the weld and buttering as well as the adjacent, exposed exterior faces of the nozzle. Convective boundary conditions were applied as before on the exposed faces of the weld and buttering as well as the top and bottom of the head.

Hydrostatic Testing and Full-load Operation

Following completion of the J-groove weld deposition steps, the hydrostatic test was simulated by ramping up the pressure on the inner surfaces of the nozzle and head to 3,125 psi and back down to zero. In the final step of the analysis, to simulate the full-load operating condition, pressure on the inner surfaces of the nozzle and head was ramped up the operating pressure of 2155 psi and the temperature of the entire model was simultaneously raised to 605°F .

Stress Results

Residual stresses are present in the region near the weld from the welding process. Under full-load operating conditions, the hoop stress in the vicinity of the downhill side of the weld on the symmetry plane is shown in Figure A.22. This stress tends to cause axial cracking. The stresses in this region are used to determine the driving force for axial crack growth. As can be seen from Figure A.22, both the weld and the buttering have yielded. Some small regions of the nozzle and the head that are in the immediate vicinity of the weld have also yielded but the stress decays quickly with distance from the weld. The axial stress in the same region is shown in Figure A.23. The axial stress is about half of the hoop stress in this region.

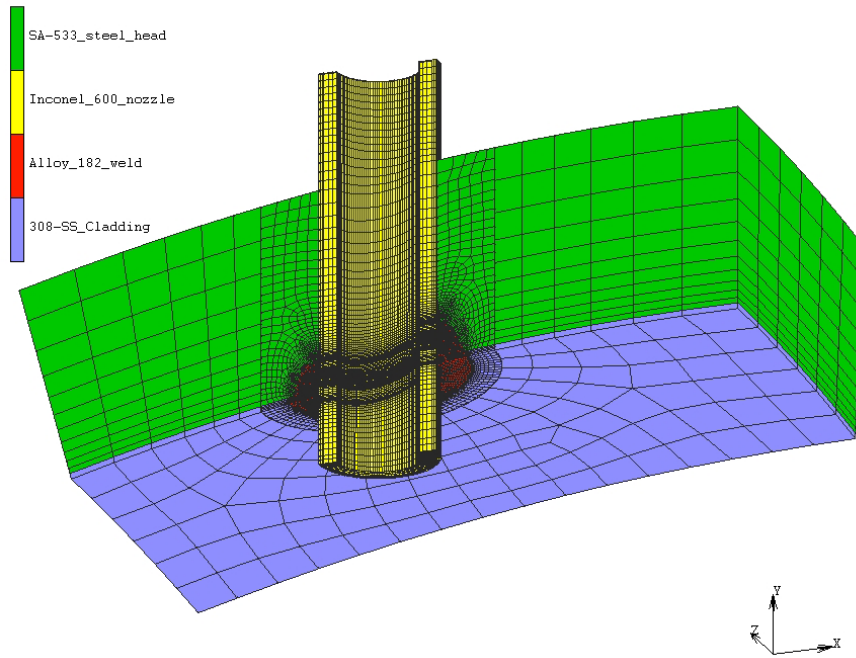


Figure A.1 Half-symmetry finite element model of Davis-Besse CRDM Nozzle-3 head penetration.

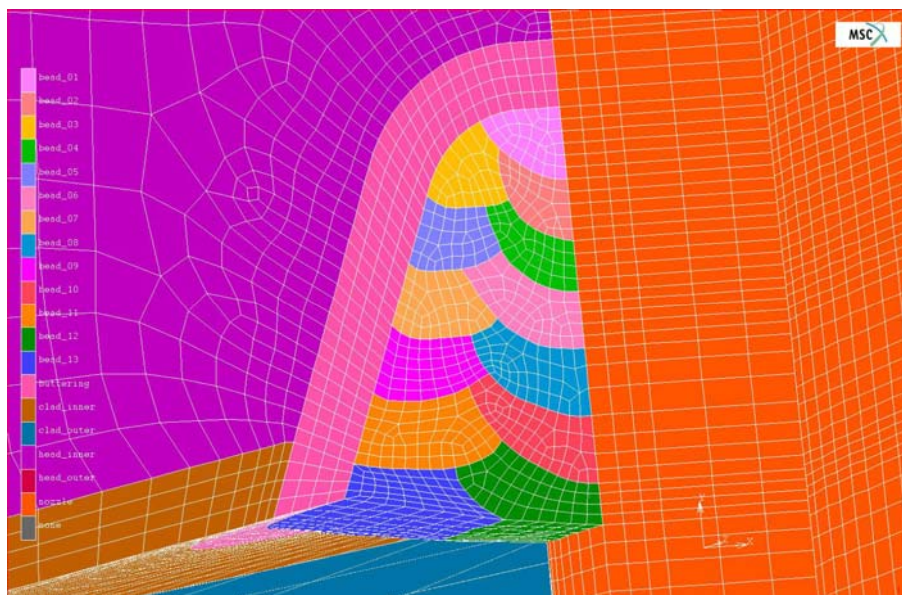


Figure A.2 Close-up view of 13-pass J-groove weld in Nozzle-3 model.

**SA-533 Gr.B Cl.1 Alloy Steel
Elastic Modulus**

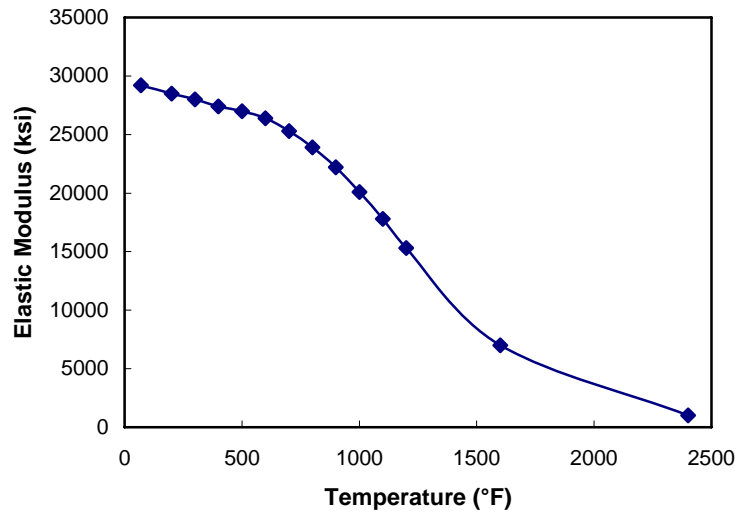


Figure A.3 Elastic modulus of ASME SA-533 Grade B Steel as a function of temperature^{7,8}.

**SA-533 Grade B Class 1 Alloy Steel
Specific Heat**

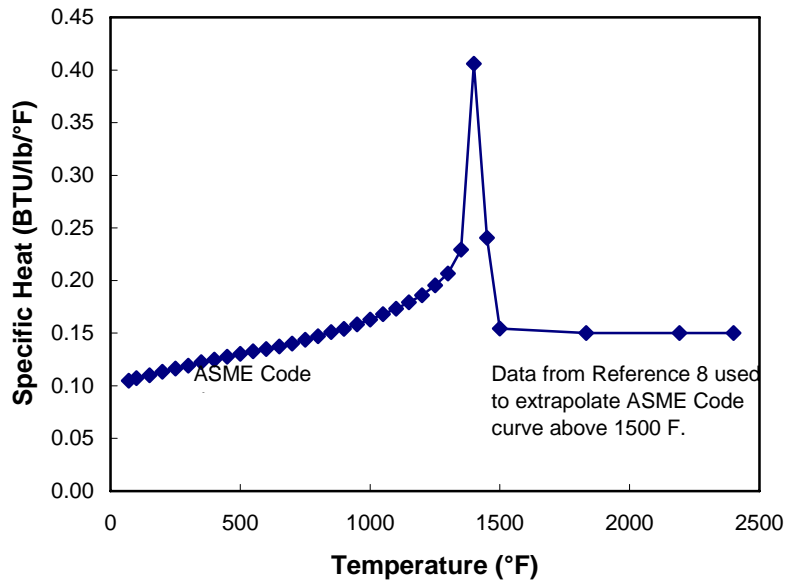


Figure A.4 Specific heat as a function of temperature for SA-533 Grade B Class 1 alloy steel ^{7,8}.

SA-533 Grade B Class 1 Alloy Steel Thermal Conductivity

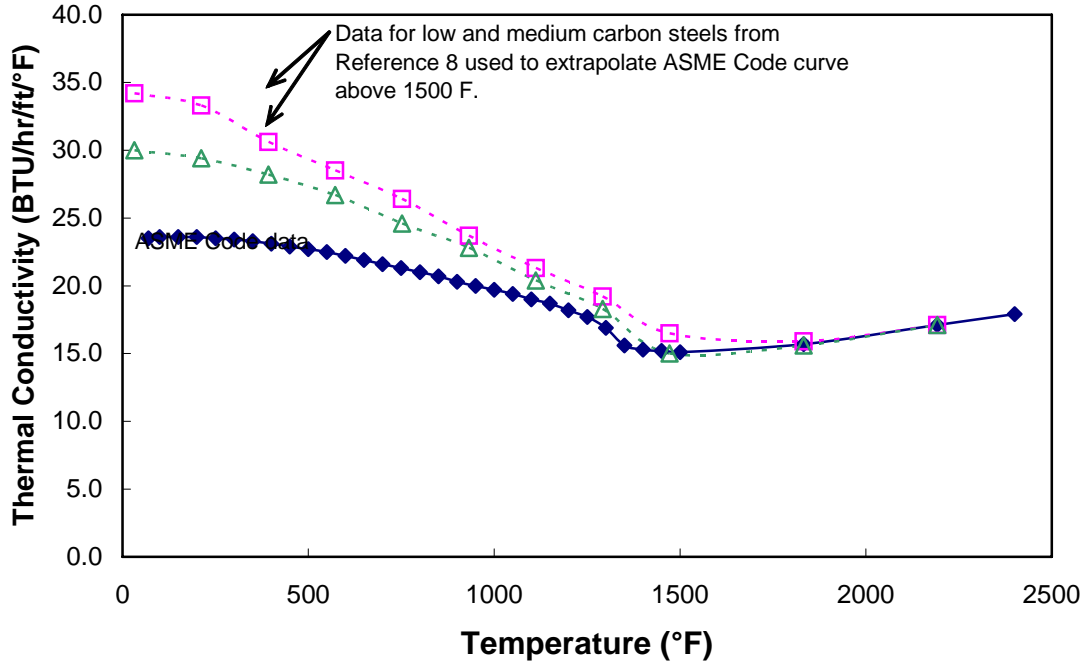


Figure A.5 Thermal conductivity as a function of temperature for SA-533 Grade B Class 1 Alloy Steel ^{7,8}.

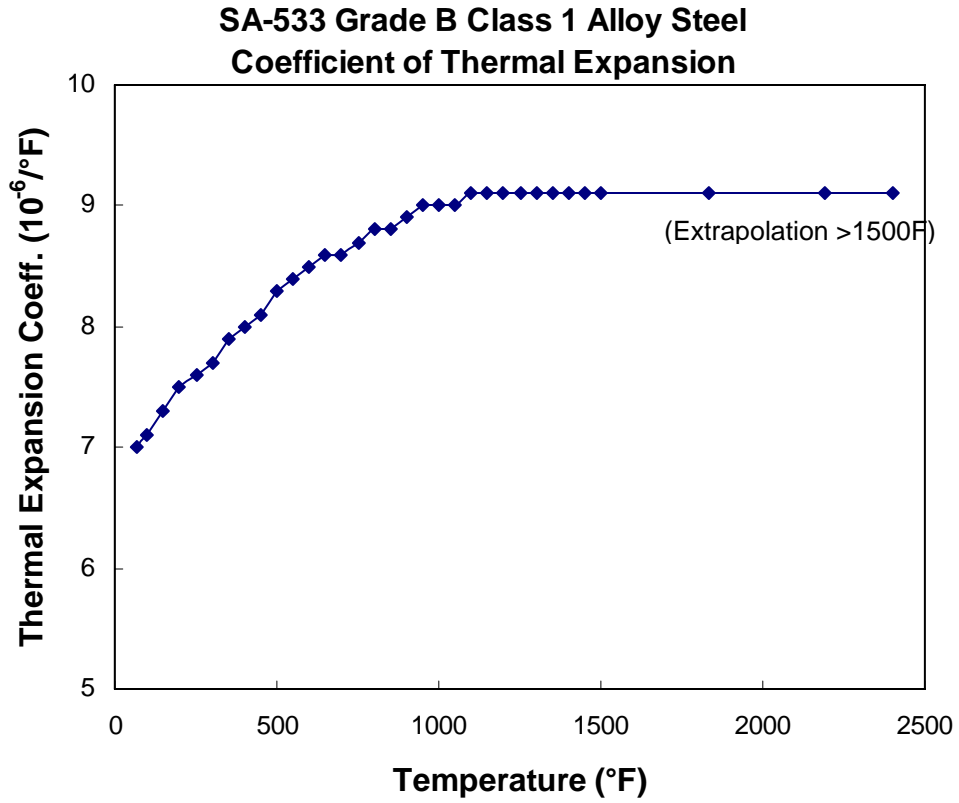


Figure A.6 Coefficient of thermal expansion for SA-533 Grade B Class 1 Alloy Steel ⁷

SA-533 Grade B Class1 Alloy Steel Yield and Tensile Strength

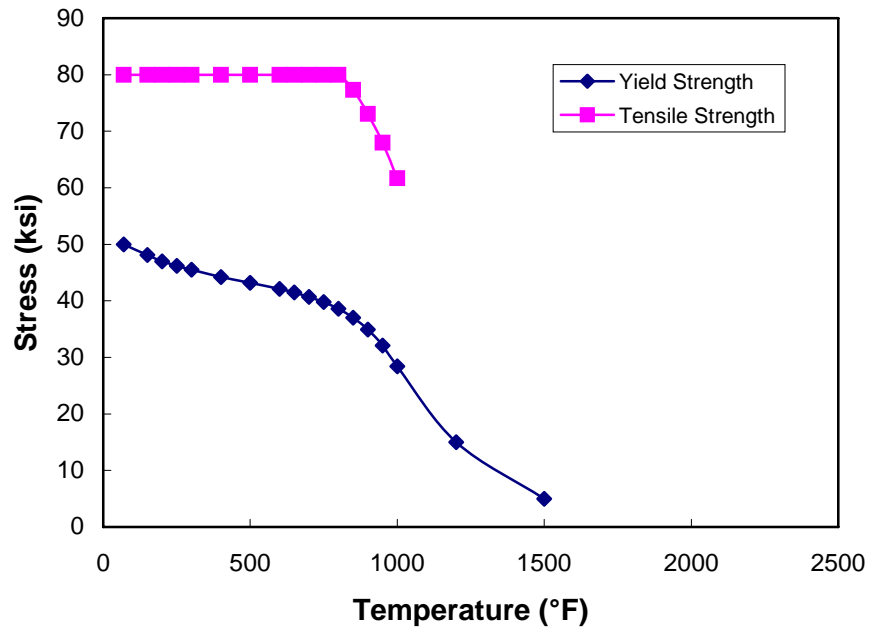


Figure A.7 Strength as a function of temperature for SA-533 Grade B Class 1 Alloy Steel

SA-533 Gr.B Cl.1 Alloy Steel Stress Strain Behavior

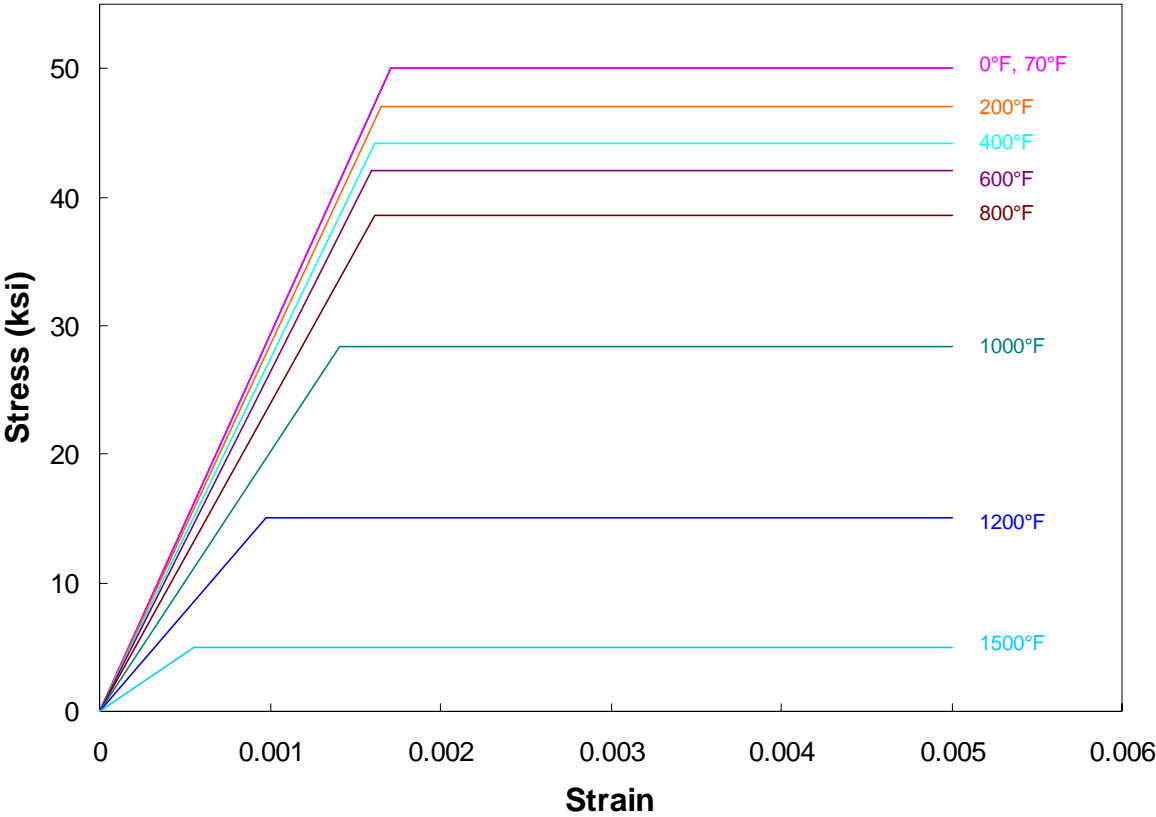


Figure A.8 Stress Strain behavior of SA-533 Grade B Class 1 Alloy Steel

Elastic Modulus Type 308 Stainless Steel Cladding

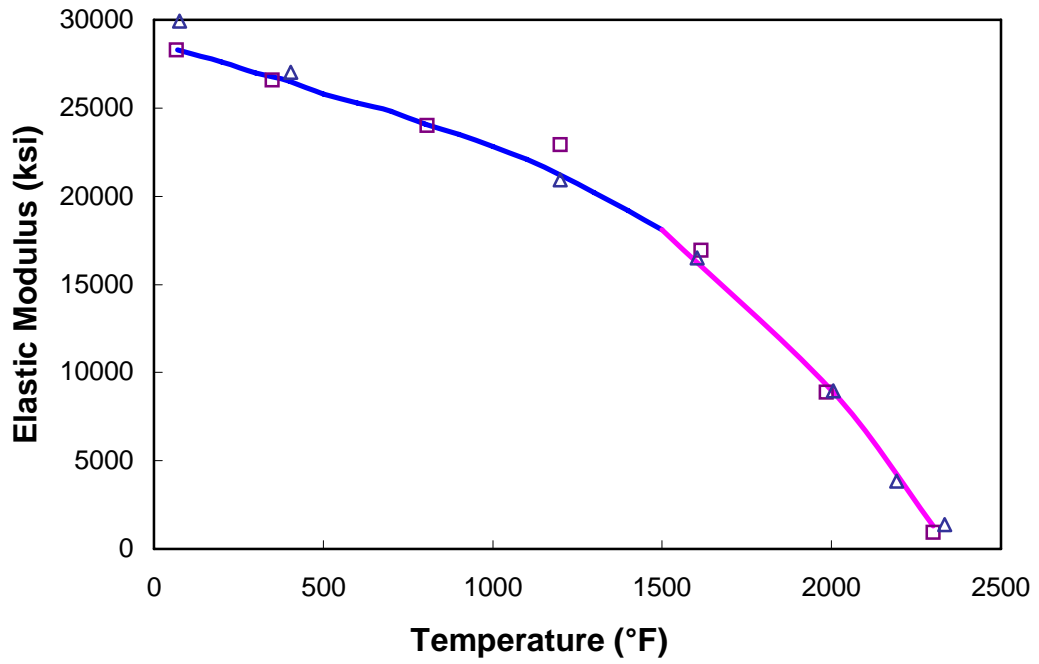


Figure A.9 Elastic modulus as a function of temperature for 308 stainless steel cladding

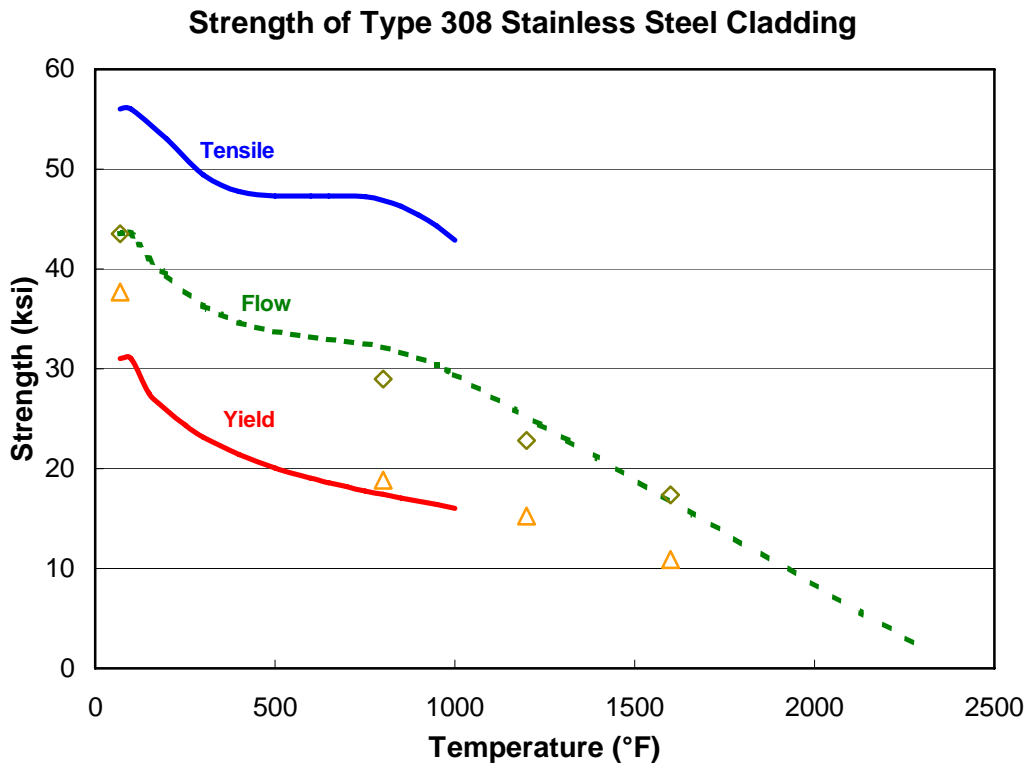


Figure A.10 Strength as a function of temperature for Type 308 Stainless Steel

Thermal Expansion of Type 308 Stainless Steel Cladding

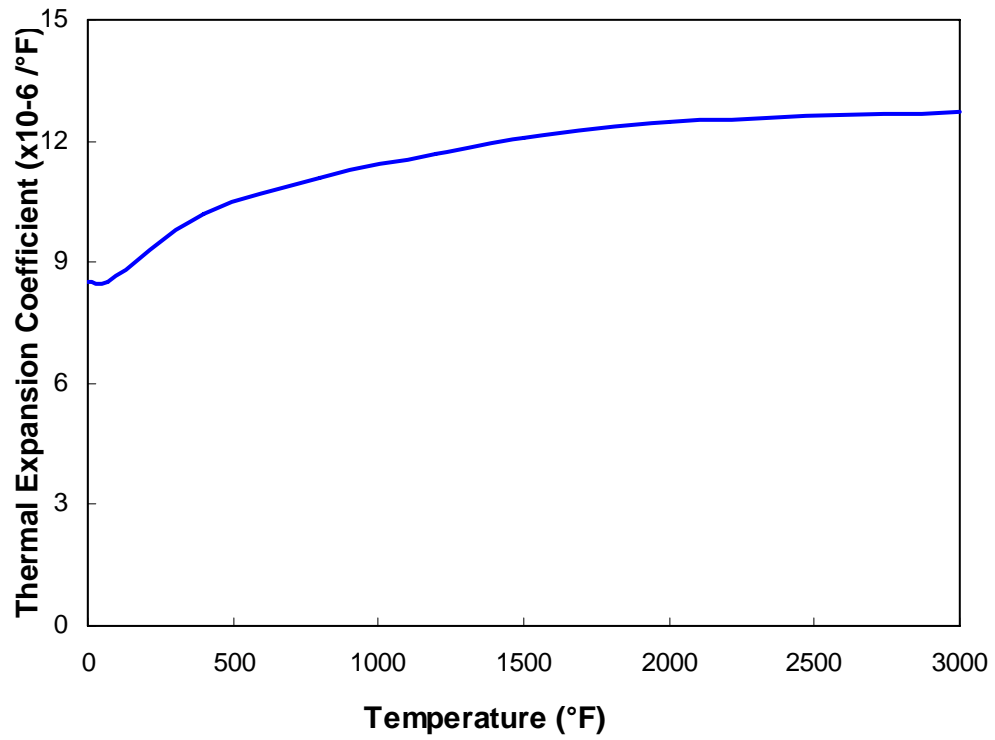


Figure A.11 Coefficient of thermal expansion as a function of temperature for series 308 stainless steel

Specific Heat of Type 308 Stainless Steel Cladding

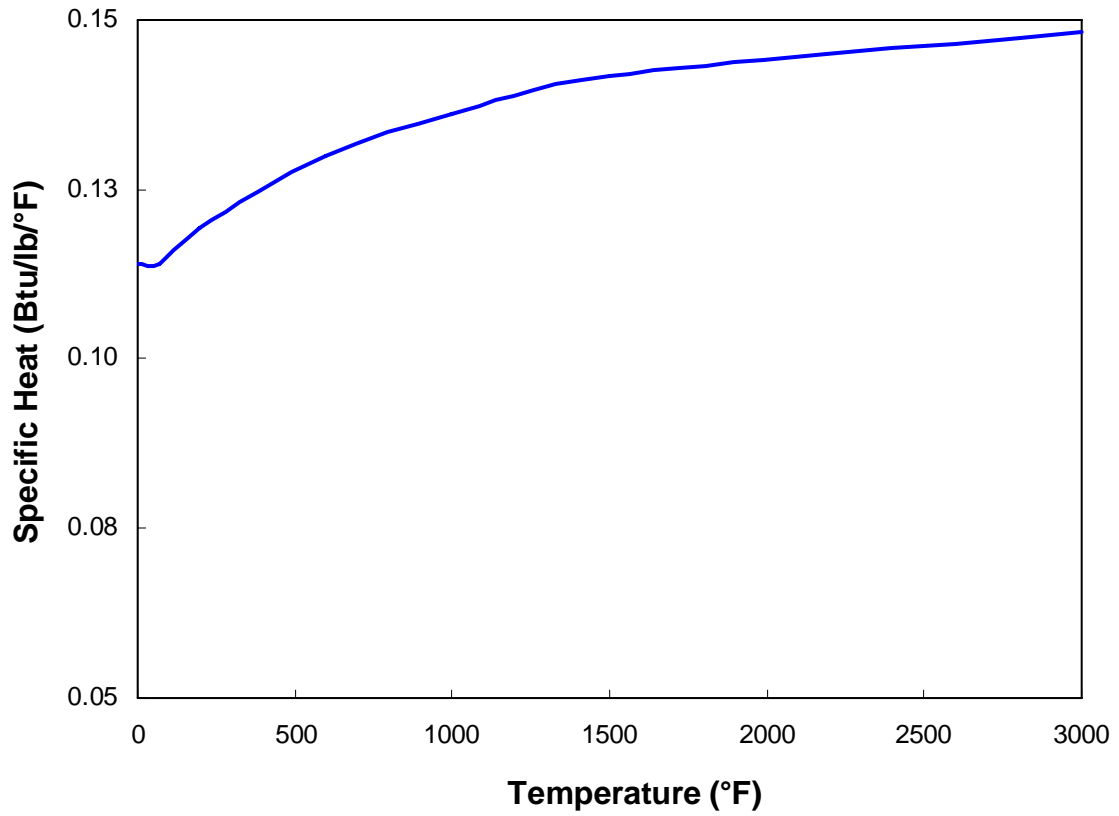


Figure A.12 Specific Heat as a function of temperature for series 308 stainless steel

Thermal Conductivity of Type 308 Stainless Steel Cladding

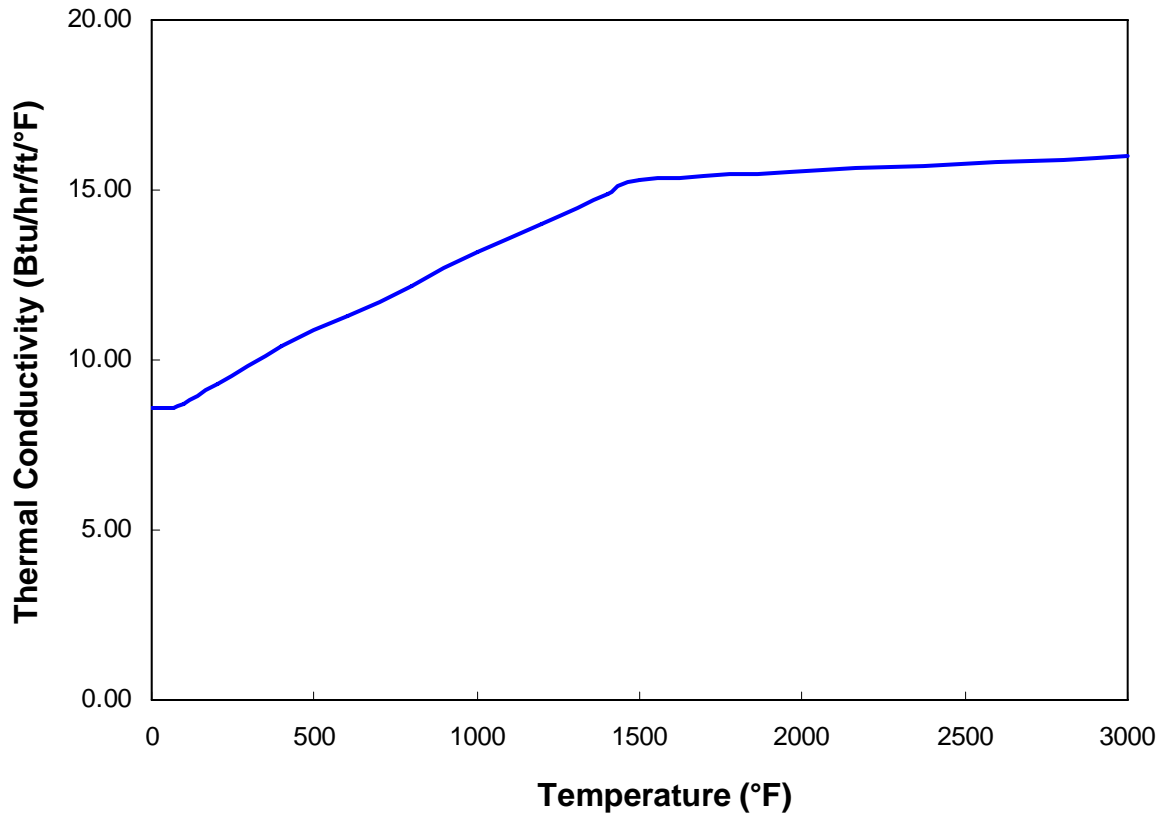


Figure A.13 Thermal Conductivity as a function of temperature for series 308 stainless steel

MA Inconel 600 Stress-Strain Data

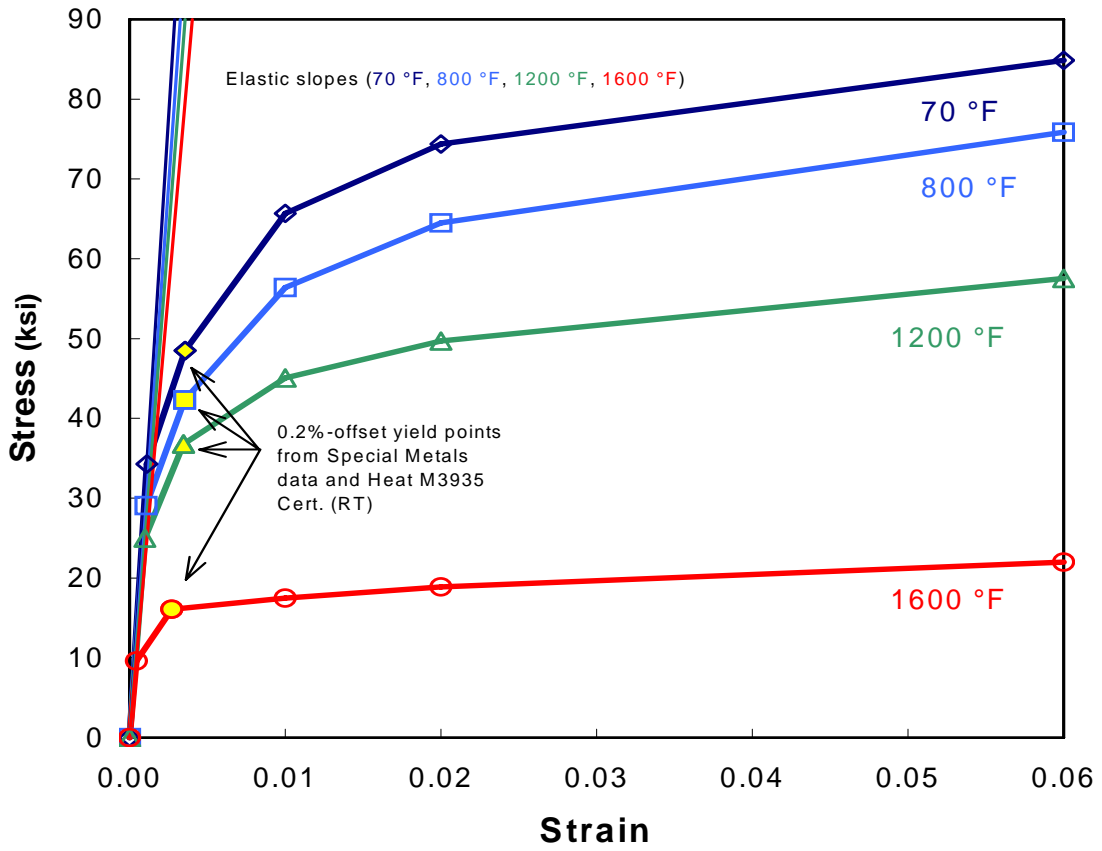


Figure A.14 Stress strain data for Alloy 600

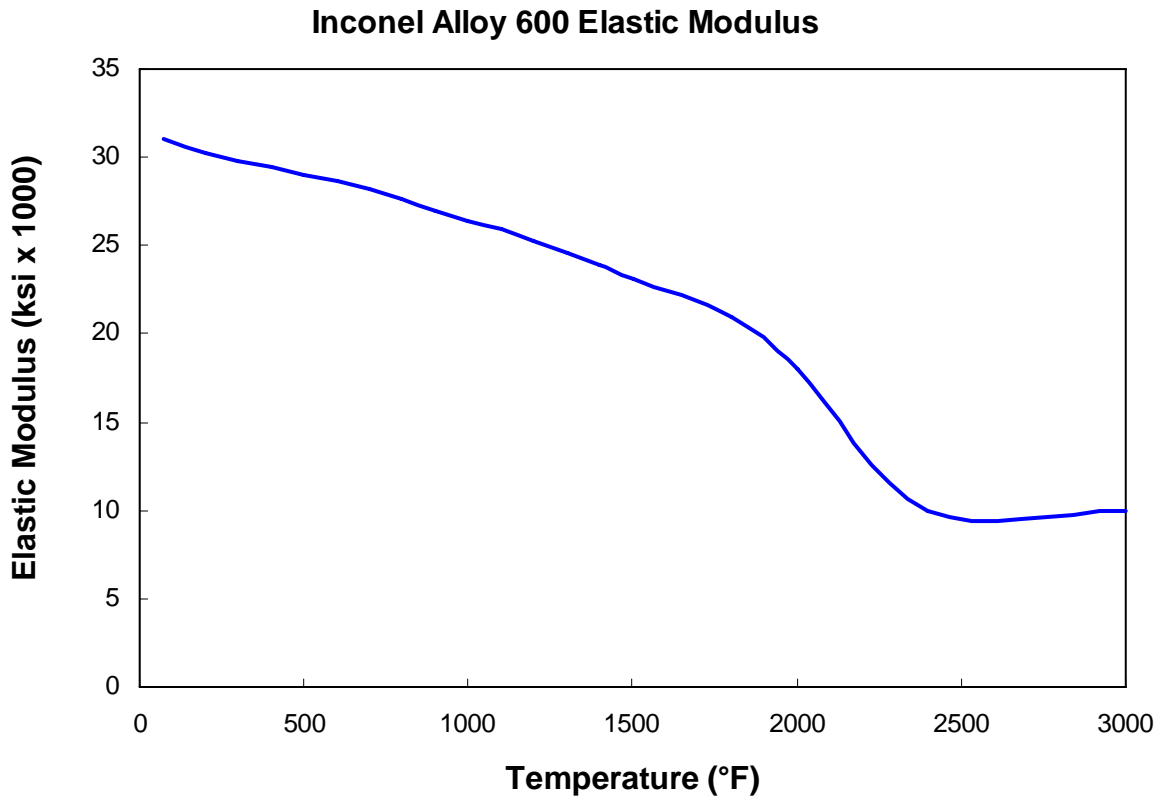


Figure A.15 Elastic modulus as a function of temperature for Inconel Alloy 600

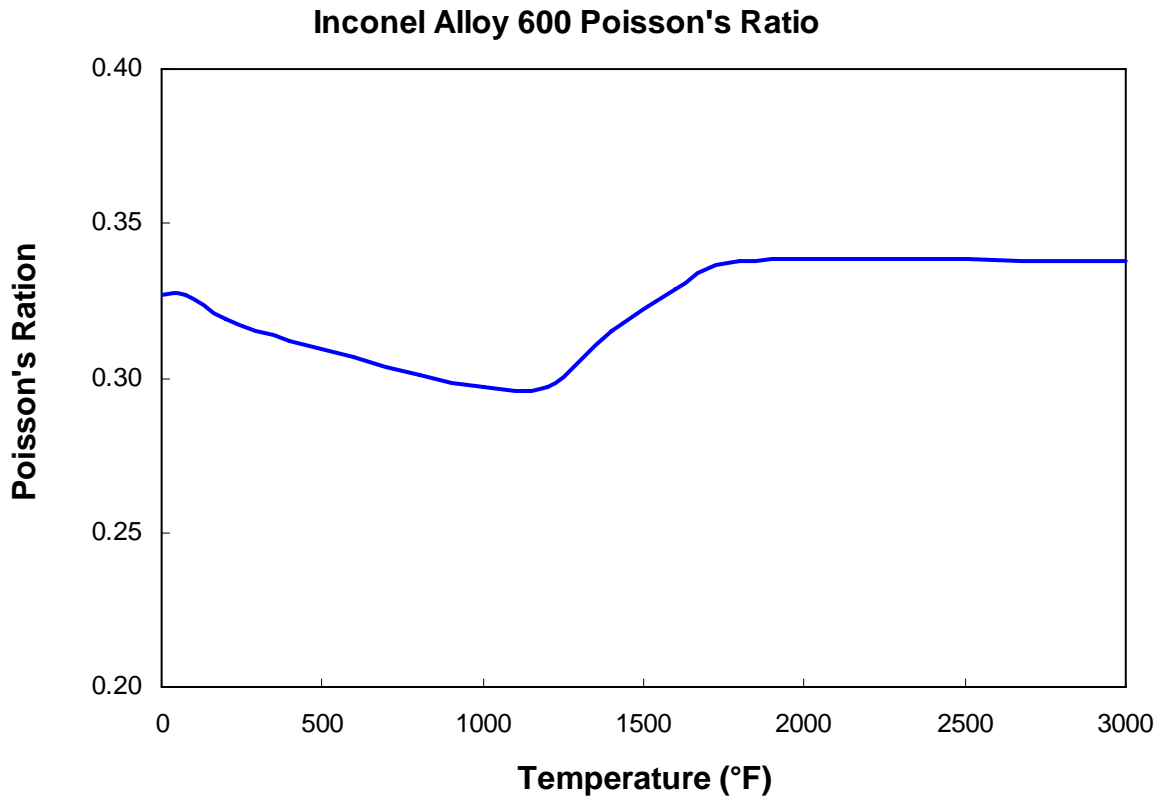


Figure A.16 Poisson's ratio as a function of temperature for Inconel Alloy 600

Thermal Expansion of INCONEL Alloy 600

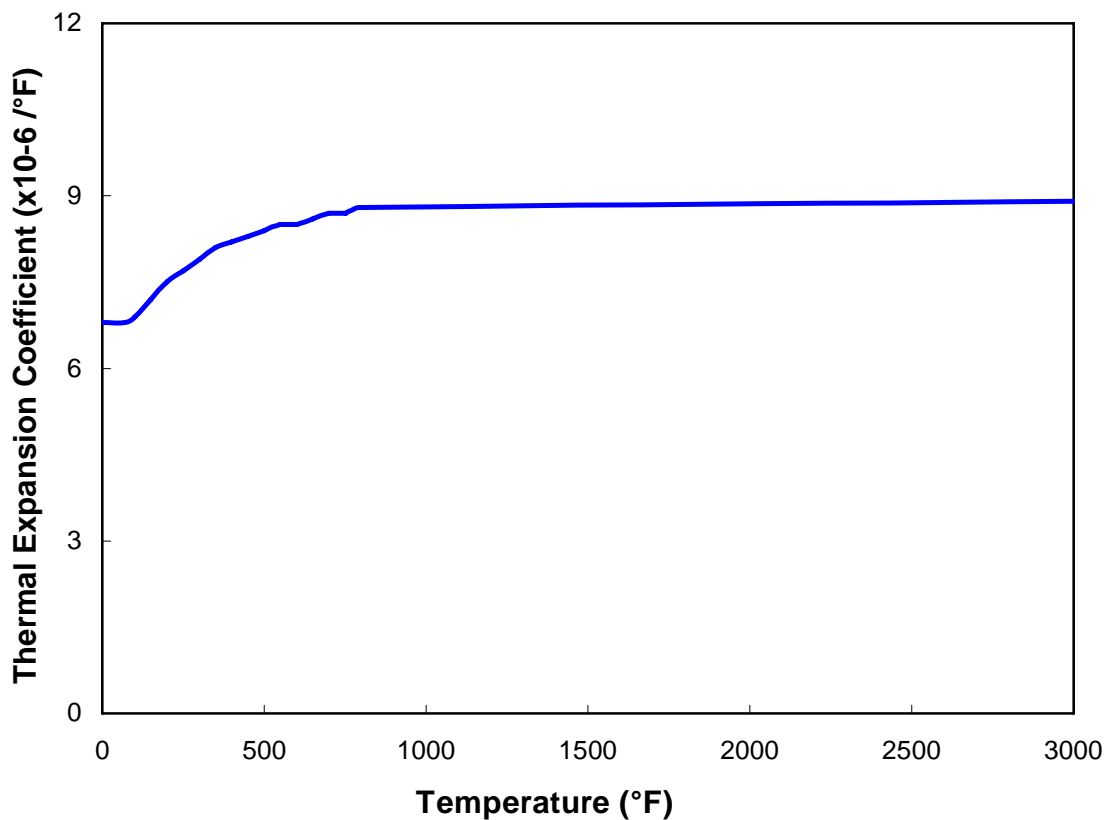


Figure A.17 Coefficient of thermal expansion as a function of temperature for INCONEL Alloy 600

Thermal Conductivity of INCONEL Alloy 600

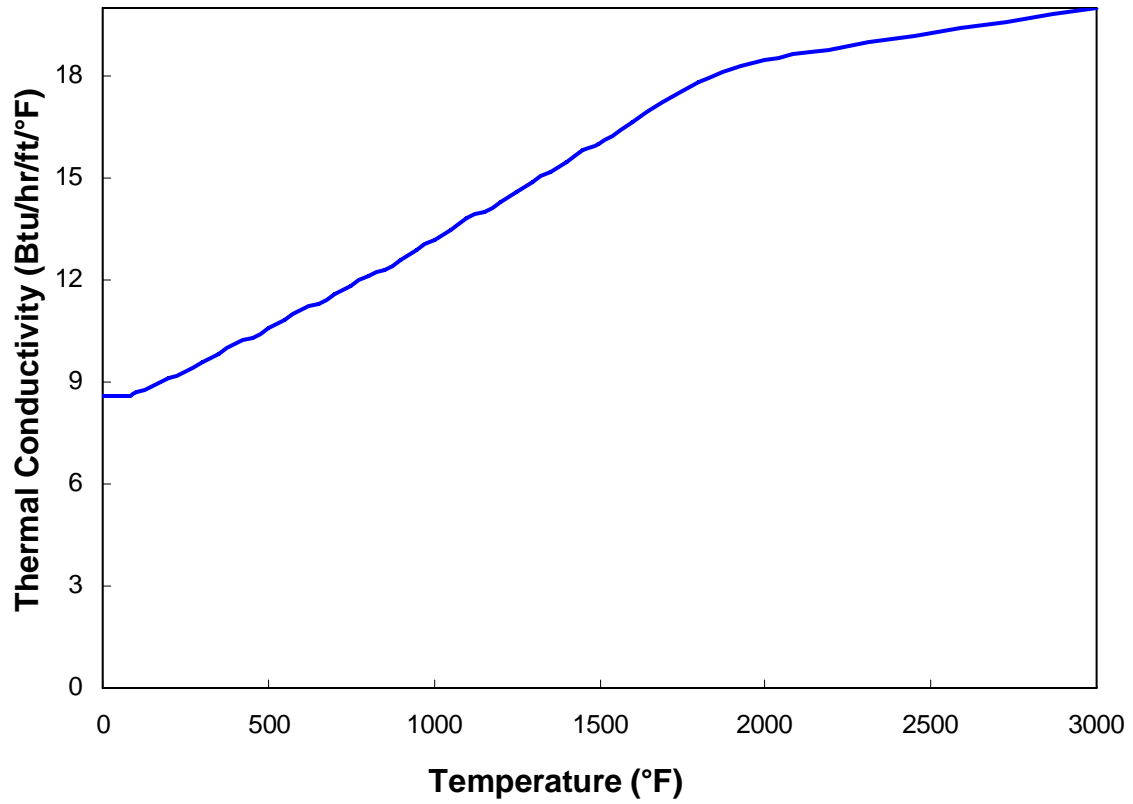


Figure A.18 Thermal Conductivity as a function of temperature for INCONEL Alloy 600

Specific Heat of INCONEL Alloy 600

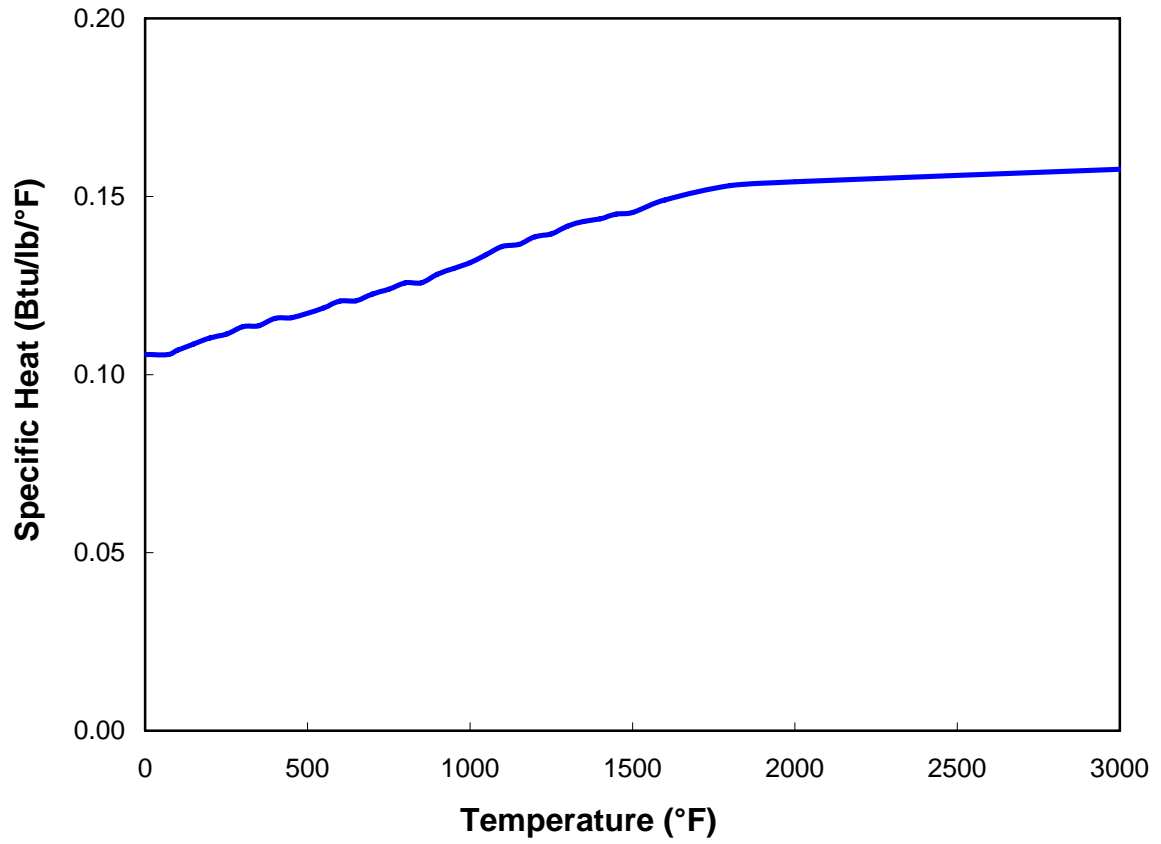


Figure A.19 Specific Heat as a function of temperature for INCONEL Alloy 600

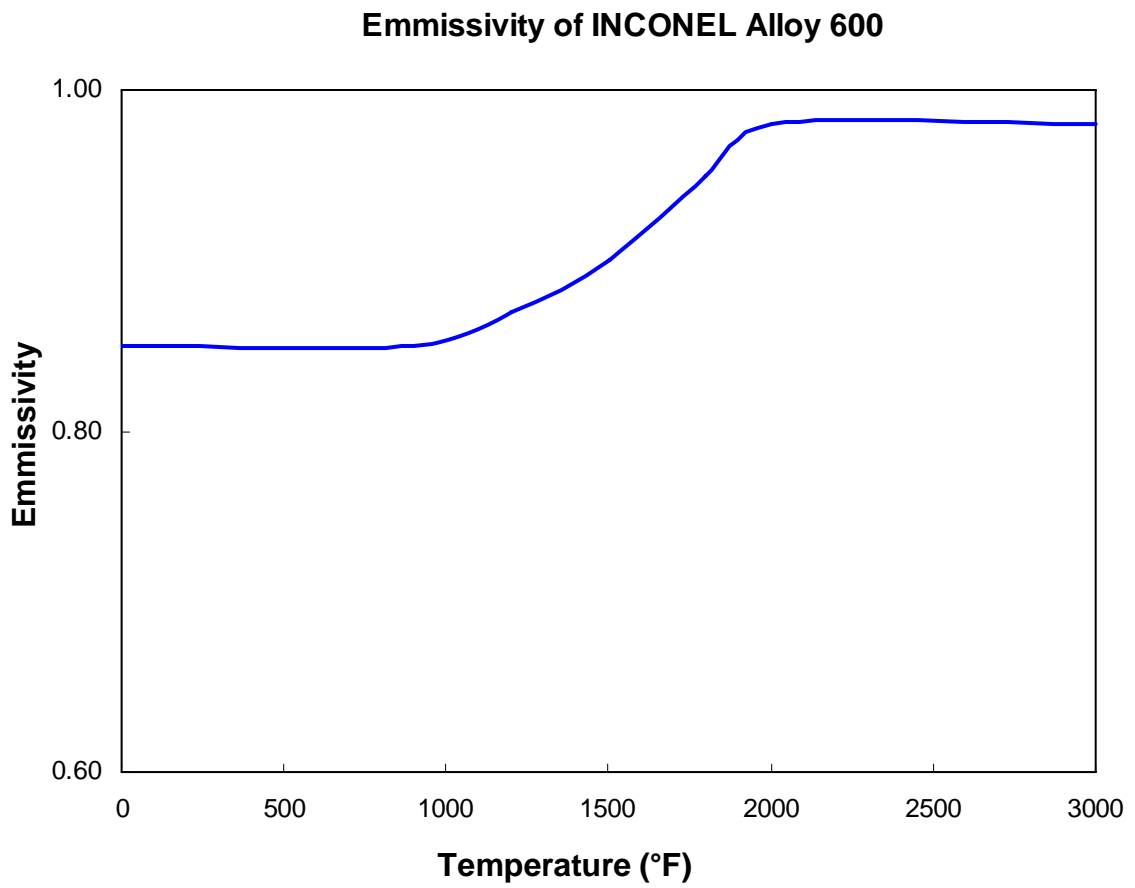


Figure A.20 Emmissivity as a function of temperature for INCONEL Alloy 600

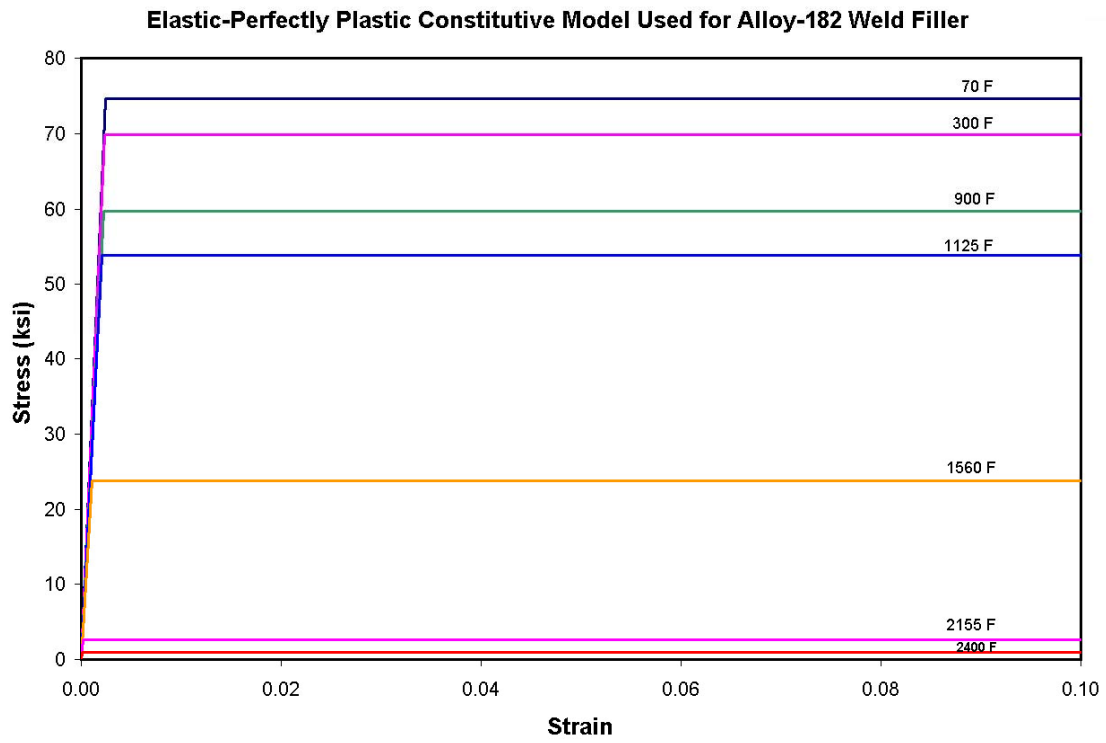


Figure A.21 Elastic-perfectly plastic stress-strain model for Alloy-182 weld filler

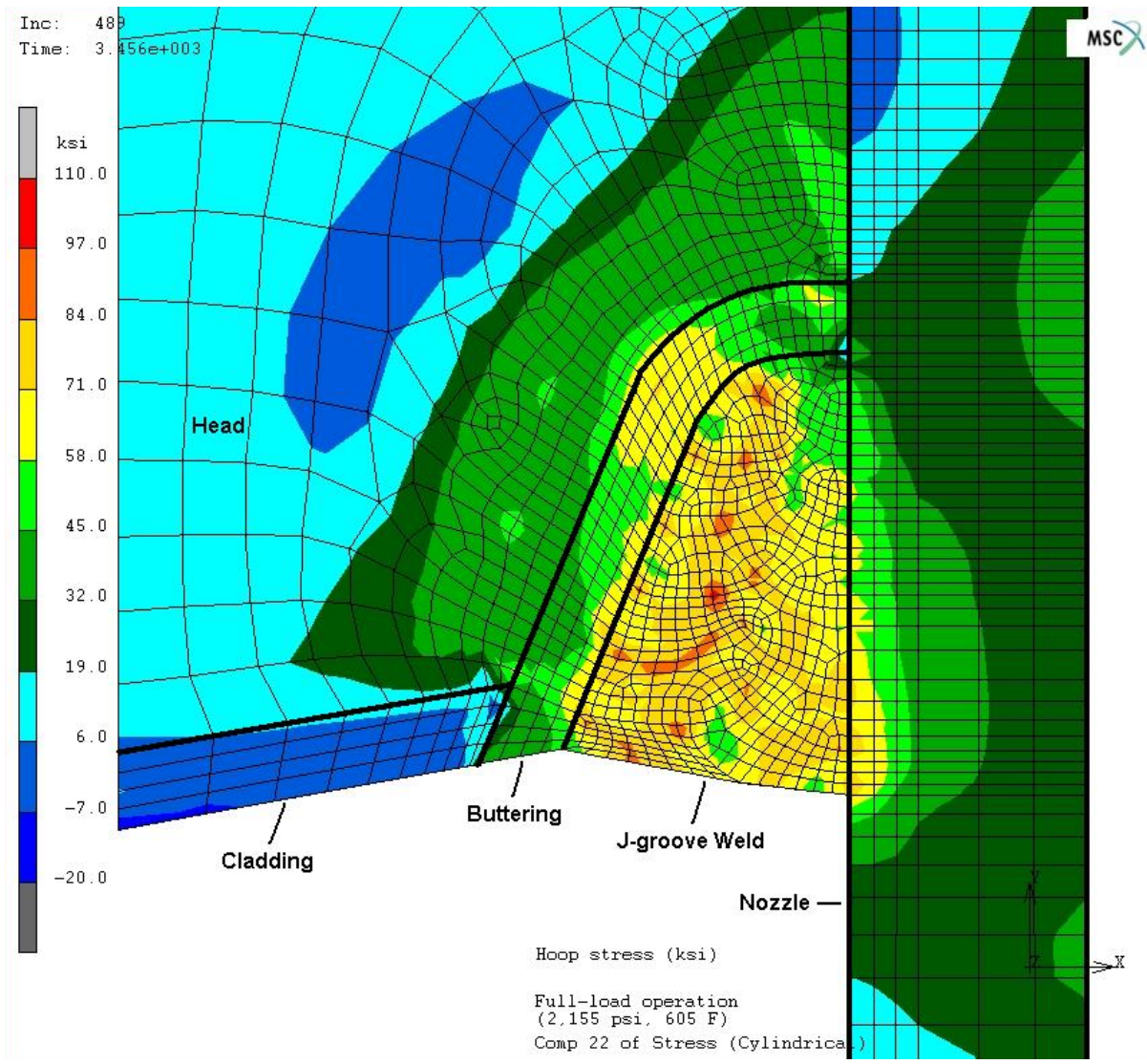


Figure A.22 Hoop stress under full-load operation

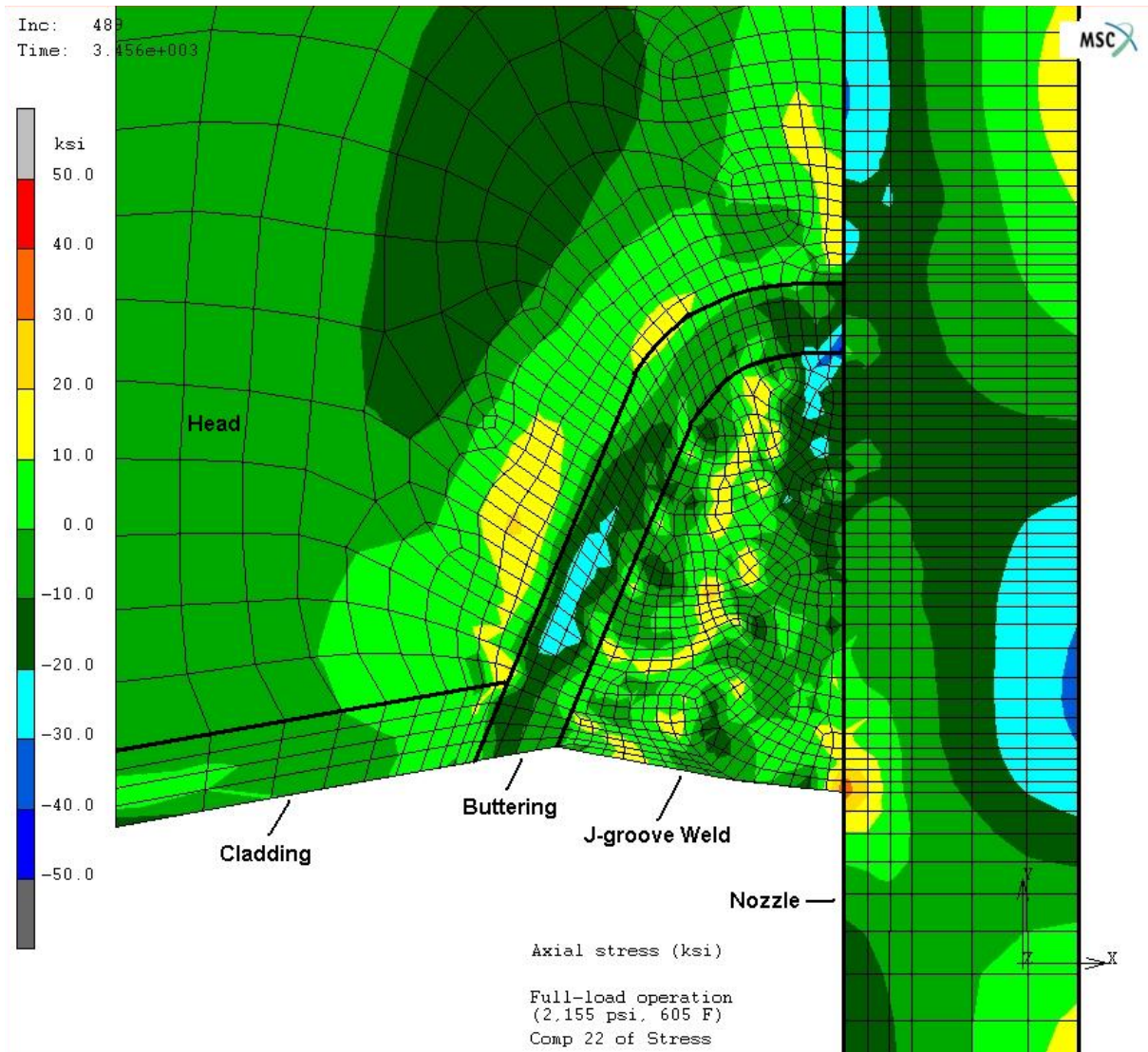


Figure A.23 Axial stress under full-load operation

References

1. “Control Rod Mechanism Housing”, Drawing No. 154632 E-R2, Babcock & Wilcox Company, May 14, 1971.
2. “Closure Head Assembly”, Drawing No. 154631 E-R4, Babcock & Wilcox Company, September 15, 1971.
3. “Closure Head Sub-Assembly”, Drawing No. 154628 E-R5, Babcock & Wilcox Company, April 12, 1978.
4. Quality Control Inspection Drawing No. 156631 E-R2, April 24, 1972.
5. Quality Control Inspection Drawing No. 154628 E-R2, March 9, 1972.
6. “Closure Head Assembly”, Drawing No. 154631 E-R4, Babcock & Wilcox Company, September 15, 1971.
7. ASME Boiler and Pressure Vessel Code, 2001 Edition, Section II, “Materials,” Part D, “Properties”, American Society of Mechanical Engineers, 2001.
8. *Structural Alloys Handbook*, 1996 Ed., CINDAS/Purdue University.